

Investigation of Normal Force and Moment Coefficients for an AUV at Nonlinear Angle of Attack and Sideslip Range

Ettore A. de Barros, *Member, IEEE*, João L. D. Dantas, António M. Pascoal, *Member, IEEE*, and Elgar de Sá

Abstract—This paper presents a comparative study of computational fluid dynamics (CFD) and analytical and semiempirical (ASE) methods applied to the prediction of the normal force and moment coefficients of an autonomous underwater vehicle (AUV). Both methods are applied to the bare hull of the vehicle and to the body–hydroplane combination. The results are validated through experiments in a towing tank. It is shown that the CFD approach allows for a good prediction of the coefficients over the range of angles of attack considered. In contrast with the traditional ASE formulations used in naval and aircraft fields, an improved methodology is introduced that takes advantage of the qualitative information obtained from CFD flow visualizations.

Index Terms—Autonomous underwater vehicle (AUV), computational fluid dynamics (CFD), hydrodynamic derivatives, maneuvering.

I. INTRODUCTION

THIS paper addresses the problem of autonomous underwater vehicle (AUV) modeling and parameter estimation with the objective of developing computational tools to predict the dynamic performance of such vehicles, thus providing solid guidelines during their design phase.

Parameter estimation methods have been used for decades in the ship building industry to predict the maneuvering performance of marine vehicles. Recently, spawned by the widespread availability of powerful computers, there has been a surge of interest in applying computational fluid dynamics (CFD) methods to construct the flow field and calculate the pressure distribution acting upon a submerged vehicle, from which the resulting forces and moments of interest acting on it can be calculated.

Manuscript received December 21, 2007; revised June 09, 2008; accepted August 11, 2008. Current version published February 06, 2009. This work was supported in part by the FAPESP foundation, São Paulo, Brazil and by the FCT-ISR/IST Pluriannual Program with POS C/FEDER funds, the Maya Project with the AdI, and the Indo-Portuguese Cooperation Program.

Associate Editor: H. Maeda.

E. A. de Barros and J. L. D. Dantas are with the Department of Mechatronics, University of Sao Paulo, CEP 05508-900, São Paulo, SP, Brazil (e-mail: eabarros@usp.br; dantas.joao@gmail.com).

A. M. Pascoal is with the Institute for Systems and Robotics (ISR) and the Department of Electrical Engineering and Computers, Instituto Superior Técnico (IST), 1049-001 Lisbon, Portugal (e-mail: antonio@isr.ist.utl.pt).

E. de Sá is with the National Institute of Oceanography (NIO), Dona Paula, Goa 403 004, India (e-mail: elgar@nio.org).

Color versions of one or more of the figures in this paper are available online at <http://ieeexplore.ieee.org>.

Digital Object Identifier 10.1109/JOE.2008.2004761

A number of authors have applied numerical tools to predict added masses, static forces and moments, and the wake field of submarines and other underwater vehicles [1]–[9]. More recently, CFD methods were used by Phillips *et al.* [10] to predict the dynamic stability derivatives of an AUV. The work of Yamamoto [11] proposes the use of CFD tools to optimize the shape of AUVs during their design phase.

Currently, the CFD approach to parameter estimation requires a considerable degree of expertise on grid generation and on the mechanization of the supporting numerical models. It also lacks experimental validation. Nevertheless, it holds great promise for the development of expedited vehicle parameter estimation methods. It is important to remark that a detailed numerical simulation of the flow field over a complete vehicle configuration is not usually justified in terms of cost/benefit for preliminary design, maneuverability, and control analysis of low to middle cost AUVs. However, CFD methods are expected to play an increasingly important role in the design of more advanced, hydrodynamically efficient AUVs.

To investigate the maneuverability of fully submerged vehicles, it is customary to represent fluid generated forces and moments in terms of coefficients, called hydrodynamic derivatives, that express the sensitivity of each force and moment to each component of the velocity and acceleration of the vehicle itself, as well as to the control surface deflections. After determining these coefficients, motion simulators can be implemented and maneuvering performance and control strategies easily evaluated. Analytical and semiempirical (ASE) methods for the calculation of hydrodynamic derivatives yield approximate results that can be used to predict maneuverability characteristics, select hydroplanes, and investigate control strategies at an early stage of vehicle design. ASE methods are directly focused on the estimation of parameters such as added mass and inertias (acceleration related coefficients), linear and nonlinear damping coefficients (related to velocities), and control action related parameters. Advanced approaches to AUV design may also involve combined plant/controller optimization, where prediction methods of hydrodynamic derivatives play an important role [12]. The ASE approach to derivatives estimation provides an analytical formulation based on physical concepts that can help in the interpretation of experimental and CFD results as well as in defining uncertainty interval for hydrodynamic parameters to help in the design of robust control systems.

The application of ASE methods to the estimation of submarine and AUV model parameters has been previously reported in the literature. See [13]–[19] and the references therein. Most of

the approaches rely on direct adaptation of methods originated in aeronautics for predicting the dynamics of aircrafts [20], [21]. However, to the best of our knowledge, no in-depth, systematic study has been done on the evaluation and validation of the above methods for AUV maneuverability prediction. As a consequence, there seems to be lacking an established approach for AUV parameter estimation allowing for the computation of the modeling errors incurred.

The ASE approach can take the benefit from specific analysis provided by the CFD simulation to adjust the formulas and improve the accuracy of estimates. Considering the usual shape of AUVs, the CFD results for critical components such as the bare hull or the lift surfaces are much less demanding of expertise and computational resources than the complete configuration of the vehicle. To establish the prediction approach, it is therefore important to combine and compare the types of estimates that are obtained with ASE and CFD methods, and to later judge the precision of those estimates by resorting to towing tank and field experiments.

This paper addresses the comparative study of ASE and CFD methods for prediction of normal force and moment for an AUV, considering the full range of angle of attack and sideslip that may occur during typical maneuvers. The vehicle predicted parameters provided by both approaches are compared to experimental results from towing tank tests. This work should be viewed as contribution to the development of efficient methods for maneuverability and control studies of axi-symmetric type of AUVs. Previous work by the authors in this direction started with the prediction of stability derivatives for the vehicle MAYA [22], [23], an autonomous vehicle that was developed under a joint Indian-Portuguese project.

The modeling of nonlinear forces and moments can be used for implementing realistic simulators and may improve the estimation of stability derivatives for maneuverability prediction and design of linear control strategies.

The axi-symmetric bare-hull geometry has been thoroughly studied, and in particular, the shape proposed by Myring [24] has been chosen for calculations and experimental validation. This geometry was adopted for vehicles such as Remus [18] and the MAYA AUV.

This paper is organized as follows. Section II presents the adopted methodology for CFD simulation, and the estimated pressure distribution and the flow characteristics in critical points of the vehicle. Section III discusses the main ASE formula proposed in the literature for estimating force and moment coefficients in the bare-hull case and for taking into account the hull-lift surface interaction. Section IV analyzes the results originated from the former approaches, comparing them to the parameters obtained in towing tank experiments. Finally, Section V provides a critical review of results obtained and indicates future steps for the research.

II. CFD SIMULATION

This section describes the results of CFD analysis of the MAYA AUV (see Fig. 1), the particulars of which are condensed in Table I.

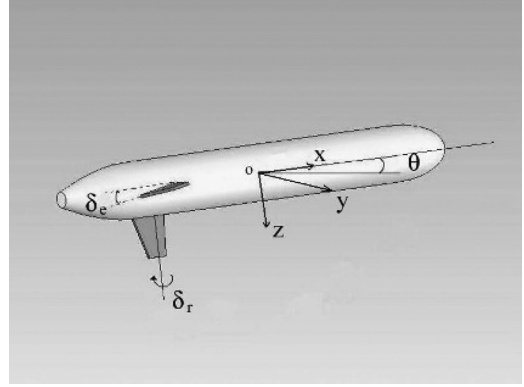


Fig. 1. MAYA AUV.

TABLE I
MAIN PARAMETERS OF THE HULL

Bare Hull Length (m)	1.742
Hull Maximum Diameter (m)	0.234
Base Diameter (m)	0.057
Nose Length (m)	0.217
Middle Body Length (m)	1.246
Myring Body Parameter θ ($^\circ$)	25
Myring Body Parameter n	2

The vehicle has a Myring-type body defined by a nose section, a middle body cylindrical section, and a tail section. The nose shape and the tail shape are described by the modified semielliptical radius distribution [24]

$$r(x) = \frac{1}{2}d \left[1 - \left(\frac{x - nl}{nl} \right)^2 \right]^{1/n} \quad (1)$$

and the cubic relationship

$$r(x) = \frac{1}{2}d - \left[\frac{3d}{2(100 - nl - cl)^2} - \frac{\tan \theta}{(100 - nl - cl)} \right] (x - nl - cl)^2 + \left[\frac{d}{(100 - nl - cl)^3} - \frac{\tan \theta}{(100 - nl - cl)^2} \right] (x - nl - cl)^3 \quad (2)$$

respectively, where x is the axial distance to the nose tip, d is the maximum hull diameter, nl is the nose length, cl is the middle body length, and θ , the Myring parameter, is the tail semiangle.

From the 2-D profile defined above, the body of revolution is generated. The solver adopted in CFD simulations is the Fluent 6.2, using the “ $k - \omega$ shear stress transport” turbulence model. Taking such model into account in the grid generation, the near-wall (i.e., close to the hull surface) modeling method defines the minimum spacing between grid elements to achieve y^+ , representative of the local Reynolds number, as close to 1 as possible [25]. This parameter is defined as

$$y^+ = \frac{yu_*}{\nu} \quad (3)$$

where y is the distance to the body surface, $u_* = \sqrt{\tau_w/\rho}$, τ_w is the shear stress at the body surface, ρ is the density of the fluid, and ν is the kinematical viscosity of the fluid.

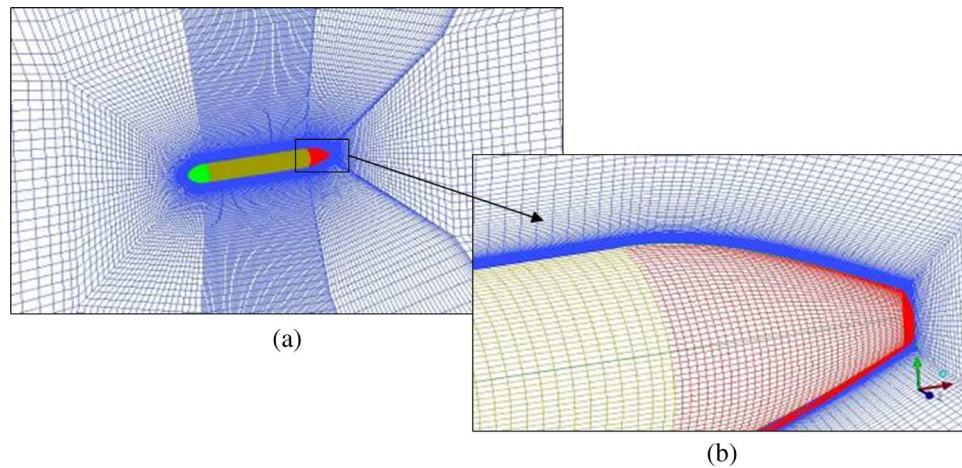


Fig. 2. Grid representation showing (a) the space closely around the vehicle and (b) the boundary layer.

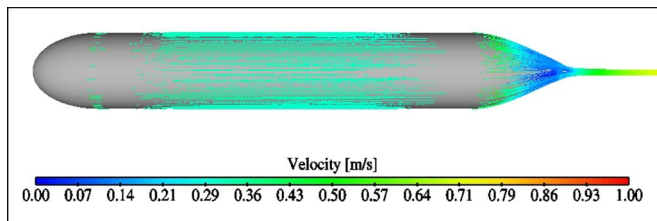


Fig. 3. Flow at zero angle of attack.

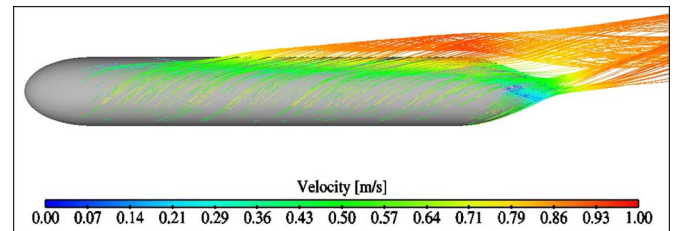


Fig. 4. Vorticity and flow separation at 20° angle of attack.

The procedure to define the spacing between grid elements adopted as a starting point the boundary layer thickness distribution for the Myring geometry calculated in [26]. The maximum value of the boundary layer thickness was adopted as the height of the near-wall region, constant along the whole length of the body. The spacing was defined by dividing each longitudinal station into 40 elements, orthogonally to the body surface. The height of each element was gradually increased from the surface to the boundary layer end. At the stern, where the viscous effects are more important, the density of the elements was increased by reducing their length. The final value of y^+ obtained was verified in the simulations, and it was close to 1 in most of the region around the body, as desired. Because the body is axi-symmetric, and subjected only to a variation in the angle of attack, a grid including just half body was considered, to save computational resources. The grid space was decomposed into three regions: a boundary layer region, the space closely around the vehicle (Fig. 2), and the outer region. All three regions included only hexagonal elements, the size of which was increased from the vehicle surface to the outer region. The outer region is a cylindrical volume. Its length is 50 times the vehicle length and the cylinder diameter is 35 times greater than the vehicle diameter.

From the simulation results, flow visualization and pressure mapping provided important information concerning the location of increased vorticity and flow separation. The increase in viscous effect with the angle of attack is clearly visible in Figs. 3 and 4. Fig. 3 shows the attached flow at zero degree of angle of attack, while Fig. 4 shows the perspective view of the vortex flow and separation that starts at the middle body for an angle of attack of 20°.

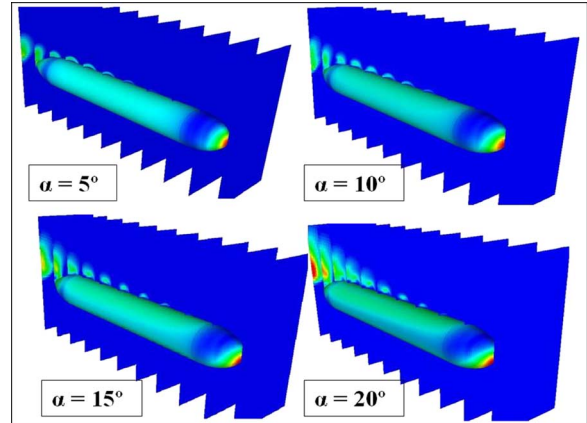


Fig. 5. Vortex distribution around the body for different angles of attack.

Fig. 5 is a visualization of the pressure distribution of the flow around the body for a range of angles of attack from 5° to 20°. Small areas over the hull representing the vortices of flow separation from the upper surface of the body can also be seen to increase in number and area, as the angle of attack is increased.

Fig. 6 shows a picture of the stern at different angles of attack. In the figure, X_0 indicates the station of the body where, as predicted by the Datcom approach [21], the flow ceases to be considered as potential. As the angle of attack is increased, it can be observed that reverse flow areas are moved to the lateral side. Even at the stern, where the viscous effects are supposed to be predominant, it is possible to identify areas (indicated by the light color streamlines) where the flow can be considered as potential.

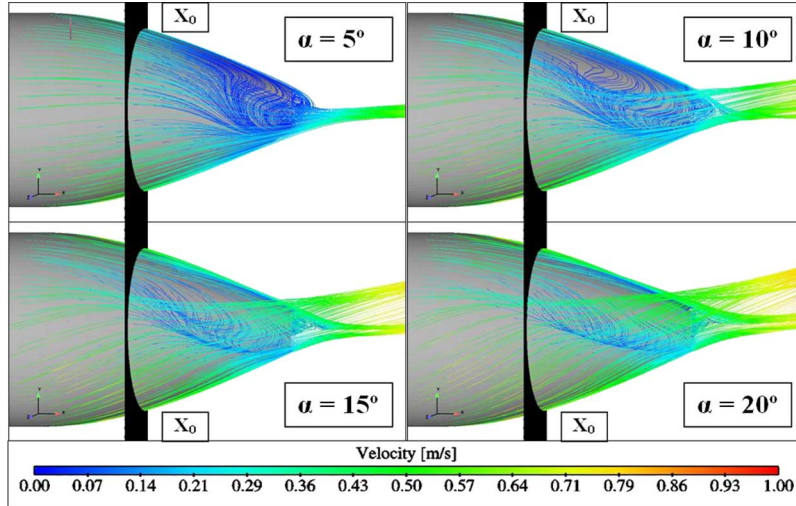


Fig. 6. Flow visualization at the stern. The station “ X_0 ” indicates the section where the flow ceases to be considered as potential according to the Datcom procedure for estimation of lift force and moment coefficients.

After validating the results, details of the flow simulation around the body and the coefficients calculated from CFD were used for adjusting the ASE formulas and combining numerical and analytical approaches for the derivatives estimation.

III. ANALYTICAL AND SEMIEMPIRICAL ESTIMATION

This section summarizes the key steps involved in the derivation of ASE formulas to estimate the hydrodynamic derivatives of a fully submerged body. The formulas used in this paper originated in the aircraft and missile related literature [27] but were properly modified to include the results of research work in the marine field, namely, in what regards the study of rudder influence on ship maneuverability [28]. They can be applied to predict the hydrodynamic derivatives of a large class of AUVs with conventional, streamlined bodies of revolution.

A. Bare-Hull Coefficients

In the Allen–Perkins [29] model, the cross-flow lift attributed to viscous cross-flow separation is added to the lift predicted by potential flow theory. The potential lift term adopted is the one derived by Munk [30] for the cross force per unit of length, given by

$$f_p = (K_2 - K_1)q_\infty \sin 2\alpha \frac{dS}{dx} \quad (4)$$

where S is the cross-sectional area of the body at the axial distance x from the nose tip, α is the angle of attack, and q_∞ is the free stream dynamic pressure. The coefficients K_1 and K_2 are, respectively, the longitudinal and transverse apparent mass coefficients for the body. The difference $(K_2 - K_1)$ is close to unity for slender bodies.

For supersonic flow, the classical work of Ward [31] has showed that the cross force at small angles of attack acts at an angle midway between the normal to the axis of revolution of the body and the normal to the free-stream velocity (i.e., at an angle $\alpha/2$). Thus, the formula in (4) would be multiplied by $\cos(\alpha/2)$ in this case. This result has been adopted by the missile community even for the subsonic flow [27], [29]. In this

paper, however, the simpler expression for the normal force derived by Munk and by the subsonic slender body theory is adopted [32].

For the cross-flow lift originated from viscous separation, in the case of a body of revolution with high fineness ratio, each circular cross section is treated, in the Allen–Perkins model, as an element of an infinitely long circular cylinder. The resulting viscous force per unit of length is given by

$$f_v = 2rC_{d_n}q_n \quad (5)$$

where r is the body radius at station x from the nose tip and

$$q_n = \frac{\rho V_\infty^2 \sin^2 \alpha}{2} \quad (6)$$

is the dynamic pressure component normal to the body axis. Parameter V_∞ denotes the free stream velocity while C_{d_n} taken as 1.2 is the steady state cross-flow drag coefficient for an infinitely long circular cylinder.

Based on these considerations, the proposed formula for the normal force coefficient $C_N(\alpha)$ is given by

$$C_N(\alpha) = C_{N_p}(\alpha) + C_{N_v}(\alpha) \quad (7)$$

where $C_{N_p}(\alpha)$ and $C_{N_v}(\alpha)$ denote the potential and viscous terms, respectively. In (7)

$$C_{N_p}(\alpha) = \frac{S_b}{S_{\text{ref}}} \sin(2\alpha) \quad (8)$$

and

$$C_{N_v}(\alpha) = \eta C_{d_n} \frac{S_p}{S_{\text{ref}}} \sin^2 \alpha \quad (9)$$

where S_b is the base area, S_p is the planform area at the xy plane (Fig. 1), and S_{ref} is the reference area (taken as L^2 in this work). The coefficient η is a correction factor, equal to the ratio of C_{d_n} for a finite length cylinder to that for an infinite cylinder. This parameter is a function of the fineness ratio L/d [21], [27], where L is the body length and d is the body maximum diameter.

The moment coefficient C_m is defined by

$$C_m = \frac{1}{L^3} \int_0^L c_N(x)(x_m - x)dx \quad (10)$$

where x_m is the axial distance from the nose tip to the center of rotation and

$$c_N(x) = \sin(2\alpha) \frac{dS(x)}{dx} + 2\eta C_d \sin^2(\alpha) r(x) \quad (11)$$

with $r(x)$ denoting the cross-sectional radius at the axial distance x from the nose tip and $S(x)$ is the corresponding cross-sectional area. From the above formulas

$$C_m = \left[\frac{V - S_b(L - x_m)}{L^3} \right] \sin(2\alpha) + \eta C_{d_n} \frac{S_p}{L^2} \left(\frac{x_m - x_c}{L} \right) \sin^2(\alpha) \quad (12)$$

where V is the body volume and x_c is the axial distance from the nose to centroid of the bare-hull planform area at xy plane.

The Allen–Perkins model yields very good results for the estimates of the normal force coefficient and produces satisfactory predictions for the moment coefficient in the case of typical missile shapes, where a long cylinder ends in a blunt base. Taking into account the smooth decrease of the cross-sectional area at the stern, which occurs also in the case of aircraft, the Datcom handbook [21] suggests that the slender body formulation of Munk should be used from the nose tip to the station X_0 of the body at which the flow can no longer be considered as potential. The semiempirical expression for the axial distance x_0 , between the nose and the station X_0 , is given by

$$x_0 = 0.378L + 0.527x_1 \quad (13)$$

where x_1 is the coordinate where the body profile has the most negative slope in the aft direction.

In the Datcom approach, the viscous contribution is considered only in the region at the stern where the flow is assumed to be entirely viscous. The formula assumes that the body lift is a simplified function of the angle of attack and is given by

$$C_L = \frac{(K_2 - K_1)2\alpha S_0}{S_{\text{ref}}} + \frac{2\alpha^2}{S_{\text{ref}}} \int_{x_0}^L \eta r(x) C_d dx \quad (14)$$

where S_0 is the sectional area at x_0 . Actually, taking as reference the Allen–Perkins model, the underlying assumption in (14) is that the angle of attack is small enough so that $\sin \alpha = \alpha$, and $\cos \alpha = 1$. Moreover, the contribution of the axial drag force to the lift is assumed negligible. Therefore, according to these assumptions, the normal force coefficient can be approximated by the lift force coefficient. The correspondent pitch moment is given by

$$(C_m)_{\text{Datcom}} = \frac{(K_2 - K_1)2\alpha}{V_{\text{ref}}} \int_0^{x_0} \frac{dSx}{dx} (x_m - x) dx + \frac{2\alpha^2}{V_{\text{ref}}} \int_{x_0}^L \eta r(x) C_d (x_m - x) dx \quad (15)$$

where S_x is the sectional area at the station x from the nose tip and V_{ref} is the reference volume for the nondimensional coefficient.

It is important to notice that the Datcom formula (11), which is based on the work of Hopkins [33], was derived by performing regression analysis on experimental data for 15 bodies of revolution. Of these, only one had geometry similar to that of a Myring body (that is, a shape that includes a cylindrical middle body). In the latter case, however, the formula derived did not provide a good approximation to the moment coefficient. The simulations by CFD suggest that a better approximation to x_0 would be aft the position calculated by the Datcom approach. In fact, as indicated by the flow visualization of Fig. 6, a significant portion of the potential term can be assumed to act over the stern of the bare hull, even when the angle of attack is increased. Moreover, the viscous contribution to the cross lift taken along the length of the hull, as in the Allen–Perkins model, seems to reproduce more accurately the nonlinear behavior of the normal force as observed in the experiments.

Motivated by the above considerations, this work proposes an improvement to the Datcom formula (14), and to the Allen–Perkins model represented by (8), (9), and (12). To keep the simplicity of the ASE approach, a modified length x_0^* was adopted as the average value between the vehicle length (used in the Allen–Perkins model) and x_0 , as calculated by (13). The modified potential term, according to this approach, is indicated by $C_{N_p}^*(\alpha)$ and the moment coefficient expression changes to

$$C_m^* = \left[\frac{V^* - S^*(x_0^* - x_m)}{L^3} \right] \sin(2\alpha) + \eta C_{d_n} \frac{S_p}{L^2} \left(\frac{x_m - x_c}{L} \right) \sin^2(\alpha) \quad (16)$$

where S^* is the cross-sectional area at X_0^* and V^* is the volume between this station and the nose tip.

B. Fin Body Interaction at the Nonlinear Sideslip Range

Considering the axi-symmetric bare-hull case, its contribution to the lateral force and yaw moment due to sideslip can be estimated by using the formulas of the preceding section. The vehicle MAYA has one fin acting as a rudder in the vertical plane. To predict its influence on vehicle maneuvering, formulas normally used for conventional aircraft and ship were initially investigated. The estimation of the lift coefficient, as a function of the angle attack, was based on the work of Wicker and Fehlner [34], who proposed semiempirical expressions similar to those adopted for ship maneuvering models [28]. The lift coefficient of a fin is calculated from

$$C_{L_F} = \left(\frac{\partial C_L}{\partial \alpha} \right)_{\alpha=0} \alpha + \frac{C_{Dc}}{a} \left(\frac{\alpha}{57.3} \right)^2 \quad (17)$$

where

$$\left(\frac{\partial C_L}{\partial \alpha} \right)_{\alpha=0} = \frac{C_{L_{2D}}}{57.3 \left[\left(\cos \Lambda \sqrt{\frac{a^2}{\cos^4 \Lambda} + 4} \right) + \frac{C_{L_{2D}}}{\pi} \right]} \quad (18)$$

is the lift slope coefficient. In the above equations, a is the effective aspect ratio, Λ is the sweep angle of the quarter-chord line,

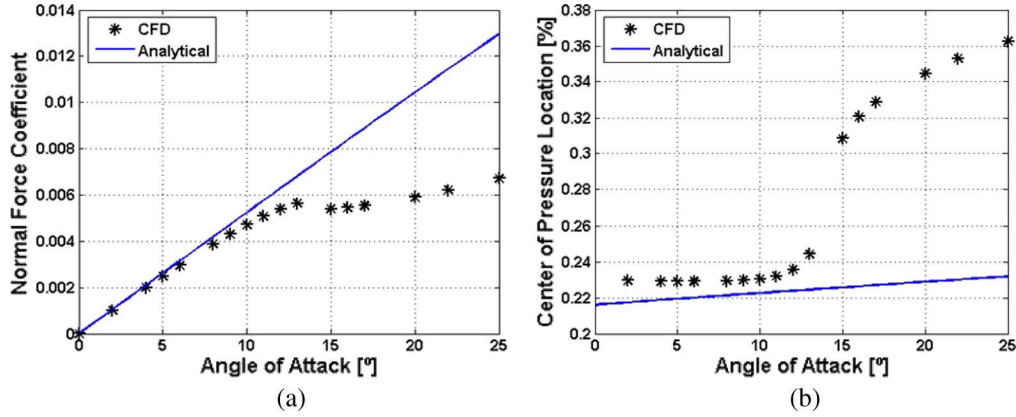


Fig. 7. CFD simulations: (a) fin alone normal force and (b) axial distance from the center of pressure to the leading edge, as a fraction of the chord length.

α is the angle of attack, $C_{L_{2D}}$ is the section lift coefficient (this value was adopted here instead of 2π , for the sake of accuracy), and C_{Dc} is the cross-flow drag coefficient (dependent on the fin shape and taper ratio)

The fin cross-flow drag coefficient is given by

$$C_{D_F} = C_{d0} + \frac{C_{L_F}^2}{\pi a e} \quad (19)$$

where C_{d0} is the minimum section drag coefficient and e is the ‘‘Oswald’’ efficiency factor; $e = 0.9$ [34]. The center of pressure of the fin is calculated from the fin moment coefficient. Taking as reference the distance from the leading edge of one fourth of middle the chord length, this coefficient is given by

$$C_{m\bar{c}/4} = \left[0.25 - \left(\frac{\partial C_m}{\partial C_L} \right)_{C_L=0} \right] \left(\frac{\partial C_L}{\partial \alpha} \right)_{\alpha=0} - \frac{1}{2} \frac{C_{Dc}}{a} \left(\frac{\alpha}{57.3} \right)^2 \quad (20)$$

where

$$\left(\frac{\partial C_m}{\partial C_L} \right)_{C_L=0} = \frac{1}{2} - \frac{1.11 [(a^2 + 4)^{1/2}] + 2}{4(a + 2)}. \quad (21)$$

From the above expressions, it follows that the longitudinal position of the center of pressure, based on the middle chord length, is given by

$$(CP)_{\bar{c}} = \left[0.25 - \frac{(C_m)_{c/4}}{(C_N)_F} \right] \bar{c} \quad (22)$$

where

$$(C_N)_F = C_{L_F} \cos \alpha + C_{D_F} \sin \alpha \quad (23)$$

is the normal force coefficient of the fin.

The formulation presented above does not take into account the low Reynolds number effect. In fact, the cruising speed adopted during the experiments and CFD simulations is 1 m/s, which corresponds to $Re = 1.32 \times 10^5$ based on the middle chord length. At this condition, stall and nonlinear effects are observed even at small angles of attack. Fig. 7 shows a comparison between the normal force coefficient obtained from (17) and (18) and the results from CFD simulations. They agree very well, in terms of the normal force coefficient, up to 7° , and around 13° , the stall is predicted only by the CFD methodology

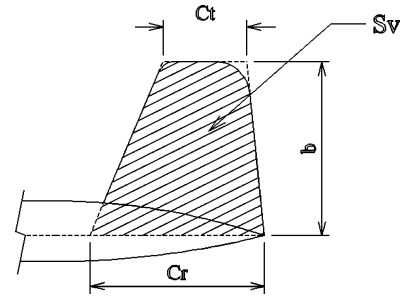


Fig. 8. Expanded fin and geometric parameters considered in the body fin interaction.

[Fig. 7(a)]. A difference is also observed in the prediction of the longitudinal position of the center of pressure [Fig. 7(b)], the longitudinal position of which was measured from the fin leading edge.

The fin–body interaction is considered next. In the ‘‘PNA model’’ (*Principles of Naval Architecture* [27]), the interference between the fin and the bare hull is considered through the effective aspect ratio, which is different from the geometric aspect ratio. Assuming that the rudder is close enough to the hull so that the cross flow over the root is negligible, the lift coefficient developed by that control surface is identical to that of a control surface of twice its geometric aspect ratio.

According to the Datcom approach, the body influence on the fin generated lift is taken into account through an increase in the effective aspect ratio and a reduction of the lift of the enlarged lift surface.

At first, considering the expanded fin surface (Fig. 8), the ratio between the effective and the geometric aspect ratio A_v is determined from the curves in Fig. 9(a), taking into account the taper ratio value ‘‘ λ_v ,’’ as a function of the span-to-the-hull-diameter ratio $2r$ of the station where the fin is fixed. The effective aspect ratio is then calculated as

$$a = f(b_v, r) A_v. \quad (24)$$

The result is then multiplied by the body–fin empirical interference factor, determined in Fig. 9(b) [21]. The final result gives the fin lift slope coefficient.

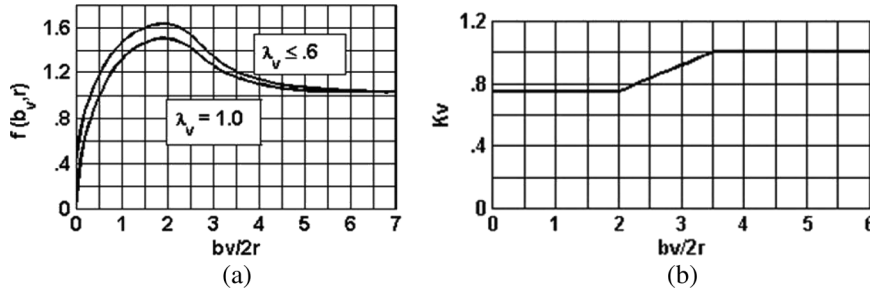


Fig. 9. Bare-hull and fin interaction: (a) effective aspect ratio and (b) empirical correction factor [21].

The Datcom prediction method seems to be more appropriate for airplanes, where the vertical fin span is large compared to the fuselage radius. According to this method, the ratio between the fin span and the body diameter shows how close the body effect is to that of an infinite plane, which makes the fin effective aspect ratio double the geometric one [see Fig. 9(a)]. The other effect of the body, obtained empirically [see Fig. 9(b)], is on the fin efficiency as a lift surface. According to the coordinate system (Fig. 1), the lateral force coefficient for the body–fin combination is then calculated by

$$(C_Y(\beta))_{BF} = -K_v(C_N)_F. \quad (25)$$

Using a different approach, rooted in the slender body hypothesis, the fin is modeled as an appendage of the hull. In this case, the influence of the bare hull on the hydroplanes is based on the added mass formulation for a slender body [35]–[38]. According to this approach, the body and fin set configuration is constructed gradually from the bare hull, adding the horizontal hydroplane, and, finally, including the vertical fin.

First, the interference from the horizontal hydroplanes on the bare hull is captured by the coefficient

$$K_{B(H)} = \frac{(m_{11})_{BH} - (m_{11})_B}{(m_{11})_B} \quad (26)$$

where $(m_{11})_{BH} = \pi \rho r^2$ is the longitudinal added mass coefficient of the horizontal tail (formed by mounting each fin on one side of a circular section, where r is the maximum hull radius at the fin location) and $(m_{11})_B = \pi \rho r^2$ is the longitudinal added mass coefficient of a circular section. This factor multiplies the bare-hull normal force coefficient. Note that the horizontal hydroplane effect onto the body lateral force $K_{B(H)}$ is zero in this case, because $(m_{11})_{BH} = (m_{11})_B$.

The interference factor from the body-horizontal hydroplane to the vertical fin is estimated according to

$$K_{F(B)} = \frac{(m_{11})_{BHL} - (m_{11})_{BH}}{(m_{11})_L} \quad (27)$$

where $(m_{11})_L = \pi \rho (s - r)^2 / 2$ is the longitudinal added mass coefficient of the lower panel mounted on a perfect reflection plane, where s is the span of the exposed fin and

$$(m_{11})_{BHL} = \frac{\pi \rho s^2}{4} \left(1 + \frac{r^2}{s^2} \right) \left[- \left(1 + \frac{r^2}{s^2} \right) + 2^{1.5} \left(1 + \frac{r^4}{s^4} \right)^{0.5} \right]$$

is the longitudinal added mass coefficient of the vertical fin added to the horizontal tail mounted on a circular section.

This factor multiplies the fin normal force coefficient to evaluate the body–fin combination in sideslip

$$(C_Y(\beta))_{BF} = -K_{F(B)}(C_N)_F. \quad (28)$$

The sideslip angle at the vertical fin is also influenced by the vortices discharged by the body. The decrease in the sideslip angle $\Delta\beta_v$ can be estimated according to the strip method formulation [39], [21]. For the range of sideslip angles considered, between -25° and $+25^\circ$, the sidewash starts to be noticed at the sideslip angle of 15° and reaches its maximum when sideslip reaches $+25^\circ$. However, the corresponding correction angle never exceeds 2.5° .

The total lateral force and yaw moment coefficients are calculated summing up algebraically body and body–fin contributions

$$\begin{aligned} C_Y(\beta) &= (C_Y(\beta))_B + (C_Y(\beta + \Delta\beta_v))_{BF} \\ &= -(C_N(\alpha))_B + (C_Y(\beta + \Delta\beta_v))_{BF} \end{aligned} \quad (29)$$

$$\begin{aligned} C_n(\beta) &= (C_n(\beta))_B + (C_Y(\beta + \Delta\beta_v))_{BF} x'_{F(B)} \\ &= -(C_m(\alpha))_B + (C_Y(\beta + \Delta\beta_v))_{BF} x'_{F(B)} \end{aligned} \quad (30)$$

where the index “B” refers to the bare hull, and “BF” refers to the contribution of the body fin combination. This last contribution can be calculated by the Datcom method [(24) and (25)], or by the “added mass” approach [(26) and (27)].

Note that the fin contribution to the moment is obtained by considering the force applied at the fin’s center of pressure. This center has a normalized longitudinal coordinate equal to $x'_{F(B)}$, determined from Fig. 7(b) and transformed according to a coordinate system at the vehicle buoyancy center, as indicated in Fig. 1. This study did not take into account a possible change in the center of pressure due to the body–fin interference.

IV. ANALYSIS OF ANALYTICAL, NUMERICAL, AND EXPERIMENTAL RESULTS

In this section, the results derived from CFD simulations and using ASE methods are compared against the normal force and moment coefficients obtained in tank tests. The AUV model was towed at 1 m/s, at different angles of attack/sideslip in the interval from -25° to $+25^\circ$. Two configurations were considered: the bare-hull model and the “T” fin set configuration (Fig. 1). The last configuration was submitted only to a variation in the sideslip angle. The coefficients are nondimensional, according to the Society of Naval Architects and Marine Engineers (SNAME) notation [40].

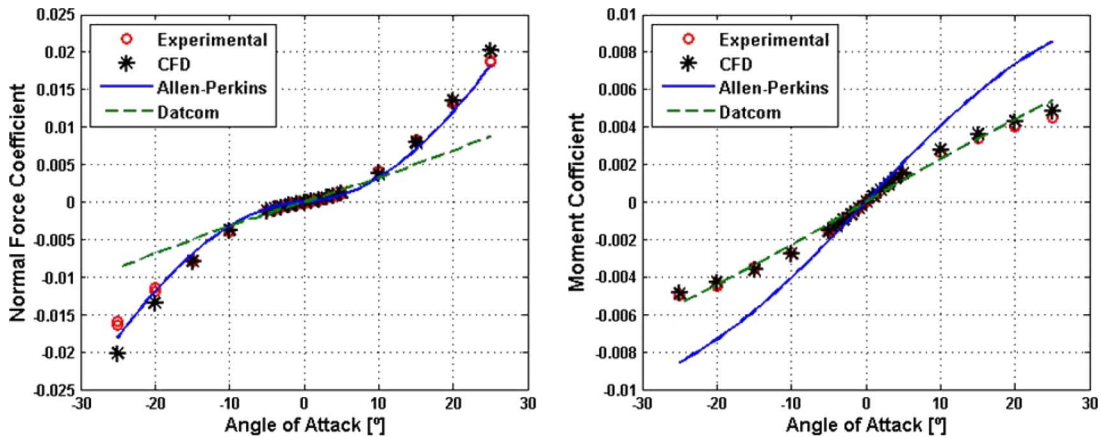


Fig. 10. Comparison among CFD calculations and ASE methods for the bare-hull case: Allen–Perkins and linear Datcom models.

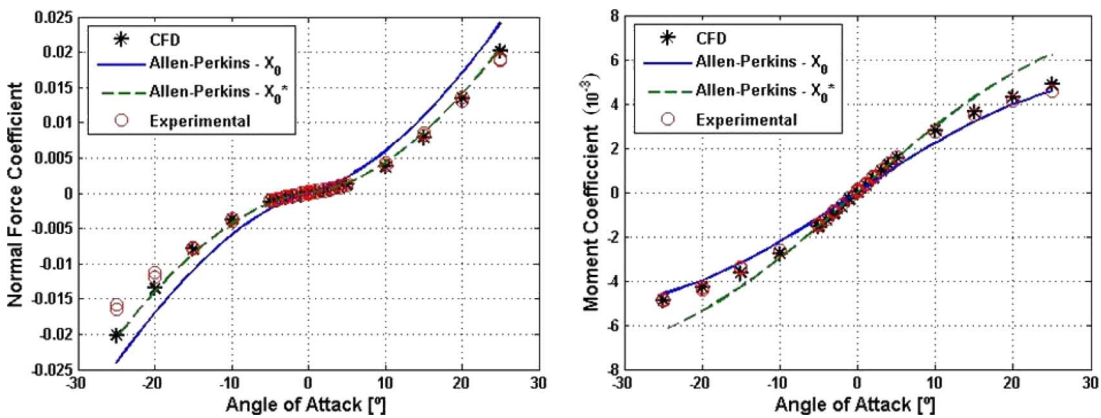


Fig. 11. Allen–Perkins model cutting the bare hull at different stations.

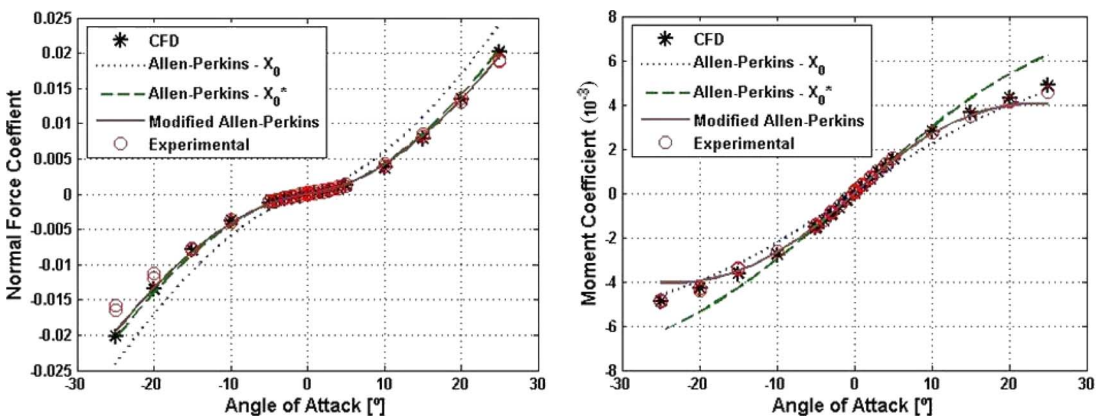


Fig. 12. Modified Allen–Perkins model for different base stations.

Figs. 10–13 show very good agreement between CFD and experimental results, thus adding credibility to the analysis based on the CFD flow visualization that was used for selecting and tuning the ASE formulas.

Fig. 10, related to the bare-hull case, includes the predicted ASE estimations according to the original Allen–Perkins model and the Datcom method. Both approaches provide similar estimations of the normal force coefficient slope. The experimental values for the moment coefficient are in between the Datcom and Allen–Perkins estimates. The effect of the small quadratic

term in the Datcom method can be observed in both graphs, as well as the poor moment slope estimate according to the Allen–Perkins approach.

The above results suggest that adapting the original Allen–Perkins model for an increase in the normal force coefficient and decrease in the moment coefficient could be achieved by adopting the Datcom suggested value x_0 for defining the location of the base station. Further improvement could be achieved by taking the qualitative information provided by the CFD visualization (Fig. 6) into account. Fig. 11

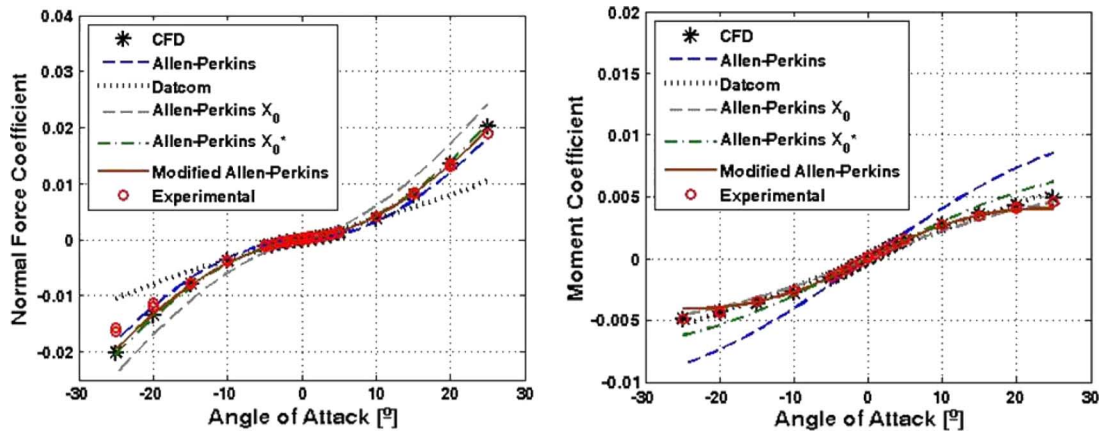


Fig. 13. Bare-hull normal force and moment coefficients using all methods tested.

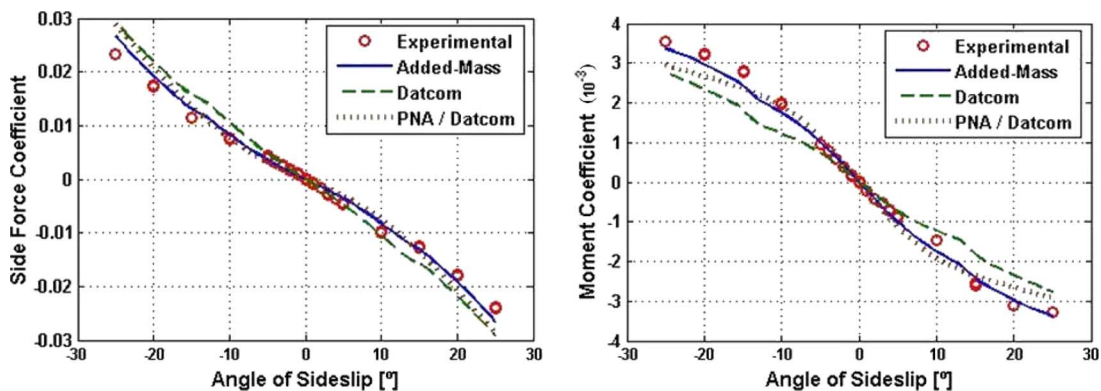


Fig. 14. Body-fin interaction using different ASE prediction methods for the fin-body interaction and mixing with the CFD result for the bare hull and fin alone.

shows the improved result in the linear range that is obtained when the base reference is changed from the station proposed according to the Datcom method to an average position between the latter and the vehicle base station. From Fig. 11, a very good prediction of the normal force and moment coefficient slopes is observed.

A final adjustment was tested for improving the agreement between the analytical and experimental results. A change in the potential term was adopted to seek a better match between experimental and the ASE predicted results for the moment coefficient, which is more sensitive to the pressure distribution along the body than the normal force coefficient. The approach is based on a correction procedure adopted in [41]. In that method, instead of cutting the vehicle at some station in the stern, the potential term is attenuated by a factor $(1 - \sin^{0.6} \alpha)$, which multiplies the boat tail contribution to the potential term in the normal coefficient term, to take into account the boundary layer thickening and flow separation at the stern. However, as observed in the CFD simulations (Figs. 4 and 5), boundary layer thickening, as well as vorticity and cross-flow separation are spread over the middle body length. The vorticity effect is likely to have its intensity increased as the angle of attack grows. This is supposed to disturb the ideal flow over the leeward side of the hull. Therefore, to take this phenomenon into account, and simplify the formula, a factor $(1 - \sin^k \alpha)$ multiplies the potential contribution over all the length of the hull. The final formula, which gives the

best agreement between ASE predicted and experimental coefficients, includes also the Munk factors

$$C_N(\alpha) = (K_2 - K_1)C_{Np}(\alpha)(1 - \sin^k \alpha) + C_{Nv}(\alpha). \quad (31)$$

The value of the exponent k that best fitted to the experimental results was chosen to be 1.3. The significant attenuation effect appears in the moment coefficient, since the viscous term disappears with $x_C = x_m$. The same factor has much smaller effect in the normal force because the viscous term dominance increases with the angle of attack. In fact, from Fig. 12, it can be observed that the force coefficient is much less sensitive to the value of k when compared to the sensitivity of C_m .

In Fig. 13, the curves produced by all the methods tested are put together. The superior performance of the Allen-Perkins model with x_0^* is clear whether in the original or in the modified form. It can also be observed that the uncertainty in the estimate of the moment coefficient considering angles of attack with amplitude greater than 10° is bounded to the interval between the estimates using x_0^* and x_0 , respectively.

Fig. 14 shows the comparison between the experimental results and the results obtained with different methodologies for predicting the fin alone and fin-body effects at sideslip. All of them include the bare-hull component $(C_n(\beta))_B$ estimated through the CFD simulation. The “PNA-Datcom” model adopted the equations (17)–(25) and the chart in Fig. 9

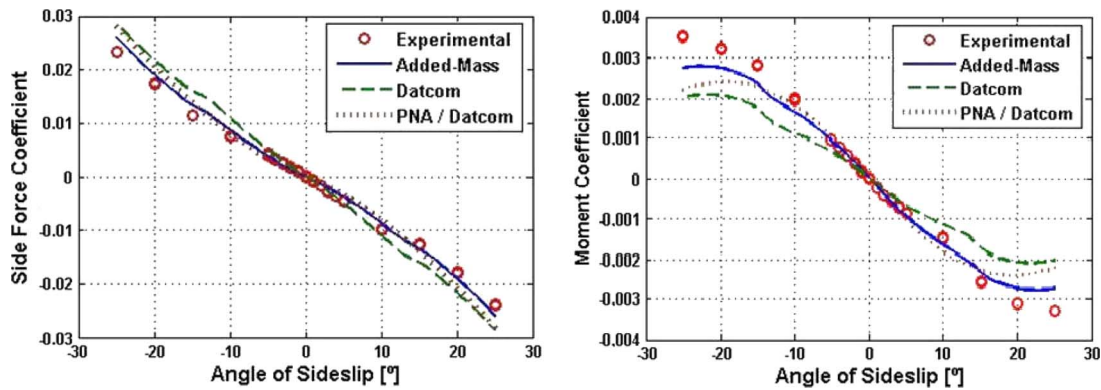


Fig. 15. Body–fin interaction using ASE prediction methods for the bare hull and the fin–body interaction, mixing with the CFD result for fin alone.

for estimating the total side force and yaw moment coefficients. The “Datcom” curve corresponds to the approach where (17)–(23) are replaced by the CFD results presented in Fig. 7, and the body–fin interference is calculated through (24) and (25). Finally, the “added mass” model uses the CFD results for the fin alone combined with (26)–(28). The stall and the more accentuated nonlinear behavior of the fin alone curves are attenuated for the combination though it is possible to observe them in both graphs of the figure for the interval between 10° and 15° . Such tendency is followed more accurately by the “added mass” model. In the first model, the lower hull–fin interference factor is compensated by neglecting the fin stall and adopting the expanded fin area in the equations. Such fortuity in the combination of results and the dominant role of the body can explain the overall performance of the “PNA-Datcom” model. A more realistic performance from the Datcom approach is probably represented by the second model, where the fin behavior represented by Fig. 7 is considered.

The tests represented by Fig. 15 change only the bare-hull component, which is estimated according to (31) and the corresponding moment equation. As expected, the performance in predicting the moment coefficient is degraded at larger angles of sideslip. Despite this, the pure ASE approach provides a satisfactory performance for most of the angles of the sideslip range.

V. CONCLUSION

This paper presented a comparative study of CFD and ASE methods applied to the prediction of the normal force and moment coefficients of the MAYA AUV. Both methods were applied to the bare hull of the vehicle and to the body–hydroplane combination.

The CFD calculations have provided very good predictions for the bare-hull normal force and moment coefficients. This makes the information given by the flow visualization and pressure distribution very useful to select or adjust the ASE formulas for predicting those parameters based on the vehicle geometry.

Unlike the case of blunt base type vehicles, the original Allen–Perkins model does not yield good estimates for the angle of attack range considered. The procedure of considering the vehicle length up to a station in between the base and that

one suggested by the Datcom approach can give better estimations for the normal force and moment slopes. The estimate uncertainty for the moment coefficient in the range of larger angles of attack is reduced when compared to the difference between the estimates provided by conventional methods such as slender body theory and Datcom.

The combination of CFD with the ASE methodology can give good cost/benefit results. This was shown by considering the very good results from CFD analysis for the bare-hull pressure distribution, which can be obtained without having to resort to intensive computations, because of the simple axi-symmetrical shape of the body. The CFD-ASE combination was important also for predicting the stall and the strong nonlinear behavior of the lift surface at moderate angles of attack. This type of information will certainly play a major role during the phase of vehicle design to meet desired open-loop performance requirements. At the same time, once bounds are known for the inaccuracies that are inherent to prediction methods, better control methods can be devised to explicitly deal in closed-loop with the uncertainties of the design models obtained.

Further investigations should consider the more conventional “+” fin configuration and the effect of the propeller duct on the vehicle hydrodynamic coefficients.

ACKNOWLEDGMENT

The authors would like to thank the Institute for Technological Research (IPT, Brazil) for the support during the tank experiments.

REFERENCES

- [1] F. Stern, Y. Toda, and H. T. Kim, “Computation of viscous flow around propeller-body configurations: Iowa axisymmetric body,” *J. Ship Res.*, vol. 35, no. 2, pp. 151–161, 1991.
- [2] S. Ju and V. C. Patel, “Stern flows at full-scale Reynolds numbers,” *J. Ship Res.*, vol. 35, no. 2, pp. 101–113, 1991.
- [3] W. G. Price and M. Tan, “Fluid forces on manoeuvring submarines and body-appendage configurations,” presented at the Int. Symp. Naval Submarines 4, London, U.K., May 11–13, 1993, Paper 3, unpublished.
- [4] I. Sahin, J. W. Crane, and K. P. Watson, “Application of a panel method to hydrodynamics of underwater vehicles,” in *Proc. 4th Int. Soc. Off-shore Petroleum Eng. Conf.*, Osaka, Japan, 1994, vol. II, pp. 406–413.
- [5] D. J. Atkins, “Computational hydrodynamics for submarines—Recent developments,” in *Proc. Warship Int. Symp.: Naval Submarines 5*, London, U.K., 1996, pp. 1–10.
- [6] D. J. Atkins, “The application of computational fluid dynamics to the hydrodynamic design of submarines,” in *Proc. Warship Int. Symp.: Naval Submarines 6*, London, U.K., 1999, pp. 1–16.

- [7] M.-S. Shin and H.-S. Choi, "Numerical simulation of the turbulent flow around a three-dimensional axi-symmetric body," in *Proc. 6th ISOPE Conf.*, Los Angeles, CA, 1996, vol. II, pp. 256–264.
- [8] D. Humphreys, "Correlation and validation of a CFD based hydrodynamic & dynamic model for a towed underwater vehicle," in *Proc. MTS/IEEE OCEANS Conf.*, 2001, pp. 1755–1760.
- [9] A. Tyagi and D. Sen, "Calculation of transverse hydrodynamic coefficients using computational fluid dynamic approach," *Ocean Eng.*, vol. 33, pp. 798–809, 2006.
- [10] A. Phillips, M. Furlong, and S. R. Turnock, "The use of computational fluid dynamics to determine the dynamic stability of an autonomous underwater vehicle," in *Proc. 10th Numer. Towing Tank Symp.*, Hamburg, Germany, 2007 [Online]. Available: <http://eprints.soton.ac.uk/48786/>
- [11] I. Yamamoto, "Research and development of past, present, and future autonomous underwater vehicle technologies," in *Proc. Int. Mater-class AUV Technol. Polar Sci.—Soc. Underwater Technol.*, Mar. 28–29, 2007, pp. 17–26.
- [12] C. Silvestre, A. Pascoal, I. Kaminer, and A. Healey, "Combined plant/controller optimization with application to autonomous underwater vehicles," in *Proc. Control Appl. Mar. Syst.*, Fukuoka, Japan, 1998, pp. 361–366.
- [13] D. E. Humphreys, "Dynamics and hydrodynamics of ocean vehicles," in *Proc. MTS/IEEE OCEANS Conf.*, 1981, pp. 88–91.
- [14] H. Maeda and S. Tatsuta, "Prediction method of hydrodynamic stability derivatives of an autonomous non-tethered submerged vehicle," in *Proc. 8th Int. Conf. Offshore Mech. Arctic Eng.*, 1989, pp. 105–114.
- [15] H. Bohlmann, "Berechnung Hydrodynamischer Koeffizienten von Ubooten zur Vohrhergabe des Bewegungsverhaltens," Ph.D. dissertation, Institut für Schiffbau der Universität Hamburg, Hamburg, Germany, 1990.
- [16] M. Nahon, "Determination of undersea vehicle hydrodynamic derivatives using the USAF Datcom," in *Proc. MTS/IEEE OCEANS Conf.*, 1993, vol. 2, pp. 283–288.
- [17] M. Nahon, "A simplified dynamics model for autonomous underwater vehicles," in *Proc. Symp. Autonom. Underwater Veh. Technol.*, 1996, vol. 2, pp. 373–379.
- [18] T. Presterio, "Verification of a six-degree of freedom simulation model for the Remus autonomous underwater vehicle," M.S. thesis, Dept. Ocean Eng. Mech. Eng., Massachusetts Inst. Technol., Cambridge, MA, 2001.
- [19] P. Ridley, J. Fontan, and P. Corke, "Submarine dynamic modeling," in *Proc. Australasian Conf. Robot. Autom.*, Brisbane, Australia, 2003 [Online]. Available: <http://www.araa.asn.au/acra/acra2003/papers/10.pdf>
- [20] S. F. Hoerner, *Fluid Dynamic Lift: Practical Information Aerodynamic and Hydrodynamic Lift*. Albuquerque, NM: Hoerner Fluid Dynamics, 1985, ISBN: 9998831636.
- [21] D. Hoak and Finck, "USAF stability and control datcom," Wright-Patterson Air Force Base, OH, 1978.
- [22] E. A. de Barros, A. Pascoal, and E. de Sa, "AUV dynamics: Modeling and parameter estimation using analytical, semi-empirical, and CFD methods," in *Proc. IFAC Control Appl. Marine Syst.*, Ancona, Italy, 2004, pp. 369–376.
- [23] E. A. de Barros, A. Pascoal, and E. de Sa, "Progress towards a method for predicting AUV derivatives," in *Proc. IFAC Manoeuvring Control Marine Crafts*, Lisbon, Portugal, 2006 [Online]. Available: http://welcome.isr.ist.utl.pt/img/pdfs/1529_C2.pdf
- [24] D. F. Myring, "A theoretical study of body drag in subcritical axisymmetric flow," *Aeronaut. Quarterly*, vol. 27, no. 3, pp. 186–194, 1976.
- [25] "Fluent 6.2 User's Guide," Fluent, Inc., 2005.
- [26] ESDU Aerodynamics, "The influence of body geometry and flow conditions on axisymmetric velocity distribution at subcritical Mach numbers," ESDU International, London, U.K., Data Item 78037, 1978.
- [27] L. H. Jorgensen, "Prediction of static aerodynamic characteristics for slender bodies alone and with lifting surfaces to very high angles of attack," NASA Tech. Rep. TR-R-474, 1977.
- [28] E. V. Lewis, *Principles of Naval Architecture*. Jersey City, NJ: SNAME, 1988, vol. III, pp. 291–308.
- [29] H. J. Allen and E. W. Perkins, "A study on the effects of viscosity on flow over slender inclined bodies of revolution," NACA Rep. 1048, 1951.
- [30] M. M. Munk, "The aerodynamic forces on airship hulls," NACA Rep. 184, 1923.
- [31] G. N. Ward, "Supersonic flow past slender pointed bodies," *Quarterly J. Mech. Appl. Math.*, vol. 2, pt. I, pp. 75–97, Mar. 1949.
- [32] K. Karamcheti, *Principles of Ideal-Fluid Aerodynamics*. New York: Wiley, 1966, pp. 568–588.
- [33] E. J. Hopkins, "A semi-empirical method for calculating the pitching moment of bodies of revolution at low Mach numbers," NACA RM A51C14, 1951.
- [34] L. F. Whicker and L. F. Fehlner, "Free-stream characteristics of a family of low-aspect ratio, all movable control surfaces for application to ship design," David Taylor Model Basin, Tech. Rep. 933, 1958.
- [35] A. E. Bryson, Jr., "Stability derivatives for a slender missile with applications to a wing-body-vertical tail configuration," *J. Aeronaut. Sci.*, vol. 20, no. 5, pp. 297–308, 1953.
- [36] A. E. Bryson, Jr., "Evaluation of the inertia coefficients of the cross section of a slender body," *J. Aeronaut. Sci.*, vol. 21, no. 6, pp. 424–427, 1954.
- [37] A. E. Bryson, Jr., "The aerodynamic forces on a slender low (or high) wing, circular body, vertical tail configuration," *J. Aeronaut. Sci.*, vol. 21, no. 8, pp. 574–575, 1954.
- [38] J. N. Nielsen, *Missile Aerodynamics*. New York: McGraw-Hill, 1960, pp. 403–416.
- [39] W. C. Pitts, J. N. Nielsen, and G. E. Kataari, "Lift and center of pressure of wing-body-tail combinations at subsonic, transonic, and supersonic speeds," 1957, Tech. Rep. NACA.
- [40] The Society of Naval Architects and Marine, "Nomenclature for treating the motion of a submerged body through a fluid," Tech. Res. Bull. No. 1-5, 1950.
- [41] ESDU Aerodynamics, "Normal force and pitching moment of conical boat-tails," ESDU International, London, U.K., Data Item 87033, 1987.



Ettore A. de Barros (M'90) was born in São Paulo, Brazil, on May 12, 1962. He graduated in engineering from the Department of Naval Architecture and Marine Engineering, University of São Paulo, São Paulo, Brazil, in 1985 and received the Doctor of Engineering degree in naval architecture and ocean engineering from the University of Tokyo, Tokyo, Japan, in 1994.

He was a Research Scientist with the Institute of Industrial Science at the University of Tokyo, from 1995 to 1996. He held visiting positions with the Control System Division of Mitsubishi Heavy Industries, Nagasaki, Japan, from 1994 to 1995, and with the Dynamical Systems and Ocean Robotics Laboratory of the Institute for Systems and Robotics (ISR), Instituto Superior Tecnico, Lisbon, Portugal, from 2003 to 2004. Since 2000, he has been Assistant Professor at the Mechatronics Engineering Department, University of São Paulo, Brazil, where he coordinates the Unmanned Vehicles Laboratory. His research specialty areas include dynamics and control of marine vehicles, and navigation systems.

Dr. de Barros is a Member of the Marine Technology Society.



João L. D. Dantas is working towards the M.S. degree in mechatronics engineering at the University of São Paulo, São Paulo, Brazil.

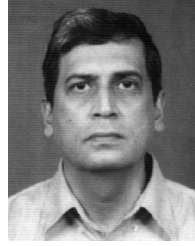
He is with the Laboratory of Unmanned Vehicles. His areas of interest include dynamics and control of marine vehicles and computational fluid dynamics.



António M. Pascoal (S'83–M'85) received the Ph.D. degree in control science from the University of Minnesota, Minneapolis, in 1987.

From 1987 to 1988, he was a Research Scientist with Integrated Systems Incorporated, Santa Clara, CA, where he worked on the development of advanced robotic systems for the U.S. Air Force and Army. He has held visiting positions with the Department of Electrical Engineering, University of Michigan, Ann Arbor, the Department of Aeronautics and Astronautics, Naval Postgraduate School (NPS), Monterey, CA, and the National Institute of Oceanography, Goa, India. He was the coordinator of two European Community (EC) funded projects [Underwater Bottom Crawler (UBC) and Self-Organizing Underwater Vehicle

(SOUV)] that led to the development of the first European civilian autonomous underwater vehicle (AUV) named MARIUS. He has been active in the design, development, and operation of autonomous underwater and surface vehicles for scientific applications, in the scope of several projects funded by the Portuguese Government, the NSF/NPS (USA), and the EC [projects: new methods for deep sea intervention on benthic laboratories (DESIBEL), Extreme Ecosystem Studies in the Deep Ocean: Technological Development (EXOCET), Advanced System Integration to Manage the Coordinated Operation of Robotic Ocean Vehicles (ASIMOV), and Coordination and Control of Cooperating Heterogeneous Unmanned Systems in Uncertain Environments (GREX)]. He is an Associate Professor of the Instituto Superior Técnico (IST, Lisbon, Portugal) and Coordinator of the Dynamical Systems and Ocean Robotics Laboratory, Institute for Systems and Robotics (ISR), IST. His areas of expertise include dynamical systems theory, navigation, guidance, and control of autonomous vehicles, and cooperative motion control of marine robots. His interests lie in the application of robotics to marine science and underwater archaeology.



Elgar de Sá was born in Kolkata, India, in 1951. He received the Ph.D. degree in physics from the University of London, Kings College, London, U.K., in 1977.

He is a Senior Scientist in the Marine Instrumentation Division, National Institute of Oceanography, Goa, India. He has number of patents and publications in the area of technology for oceanography. He has designed and developed underwater spectroradiometers, and has been actively involved in the development of the Maya AUV and in thruster driven autonomous profilers for coastal waters.